Proceedings of the 17th World Congress
The International Federation of Automatic Control
Seoul, Korea, July 6-11, 2008

Nano-Positioning of a Electromagnetic Scanner with a MEMS Capacitive Sensor

Xinghui Huang, Ju-Il Lee, Narayanan Ramakrishnan, Mark Bedillion, Patrick Chu

Seagate Technology, 1251 Waterfront Place, PA 15222, USA
(e-mail: xinghui.huang@seagate.com; juil.lee@seagate.com)

Abstract: This paper presents the control design and experimentation of a prototype electromagnetic scanner with an integrated capacitive linear and rotational position sensor for small form factor probe storage. An array of probe heads is to be precisely positioned in X/Y linear and rotation directions so that high areal density (>1 terabit/in^2) and high data throughput can be achieved. The scanner has X/Y motion capabilities with a linear stroke of about 300 μm. It can also generate rotational motion with offset actuators to compensate for disturbances, mechanical tolerance and nonlinearities. System characterization, modeling, MIMO control design and simulation, and preliminary experimental results are presented. The feasibility of rotation control with the developed capacitive sensor and offset actuators is experimentally confirmed.

1. INTRODUCTION

Compared to flash storage, probe storage technology is expected to offer ultra-high capacities and competitive data rates at reduced costs. Substantial research effort has been made to realize probe storage technology (Mamin et al. [1999], Sebastian et al. [2005]). The basic idea behind probe storage is to form bits using very small tips analogous to punch card technology but with densities in excess of 1 Tb/in^2. An array of probe tips can be employed in order to achieve high data throughputs. At a storage density of 2.4 Tb/in^2, the corresponding track pitch is about 30 nm, which requires a positioning error of less than 1.5 nm at each tip. These specifications place stringent requirements on the servo mechanical system. The lithographic challenges to make ultra-small memory cells in flash memory have now been translated to the more tractable challenges in positioning accuracy in probe devices.

This paper describes implementation of probe storage based on conventional manufacturing and assembly processes. In this implementation, a sled scanner is driven by electromagnetic actuators consisting of coil-magnet pairs, which generates linear forces in the X and Y directions and torque in the Z direction. In addition to servo marks on the media, capacitive sensors are

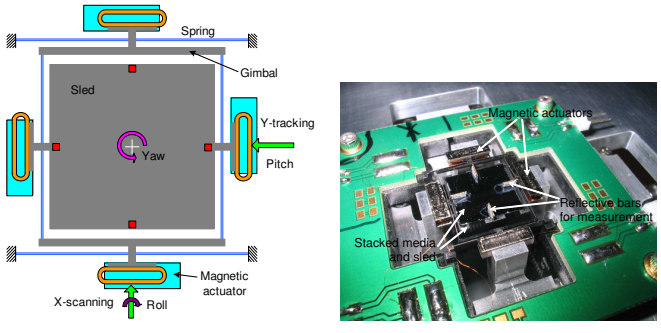

(a) (b)

Fig. 1. Sled assembly schematic and the testing fixture

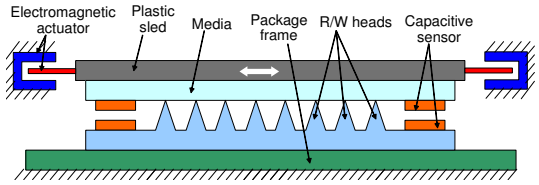

Fig. 2. Sled assembly cross-section view

formed between the static head substrate and the moving media for linear and rotational position feedback.

At any time instant, a row is chosen for simultaneous reading or writing in order to meet the data rate requirement. The head array has three in-plane degrees of freedom (DOF) including yaw, which will be referred to as rotation in what follows. When a row of heads are position-controlled simultaneously, this undesirable rotation has to be suppressed in order to achieve a small positioning error at all heads. The rotation control capability is generated by offsetting the four magnetic actuators counterclockwise from their nominal symmetric position by a small amount, so that a torque is formed in the Z direction when the actuator pair in one direction is driven differentially.

2. SYSTEM CONFIGURATION AND MODELING

The schematic view of the sled assembly is shown in Fig. 1. It has three in-plane DOFs: X-scanning, Y-tracking, and Z-yaw. Inevitably, it also has some out-of-plane modes: roll, pitch and bounce. Higher order modes are not considered here since their resonance frequencies are sufficiently high with respect to the operating frequency.

2.1 Frequency Responses

The frequency responses of the sled assembly are determined by a sweepsine measurement and are shown in Fig. 3. There are four major in-plane modes: X spring mode (X1), X gimbal mode (X2), Y spring mode (Y), and Z rotation mode (R).

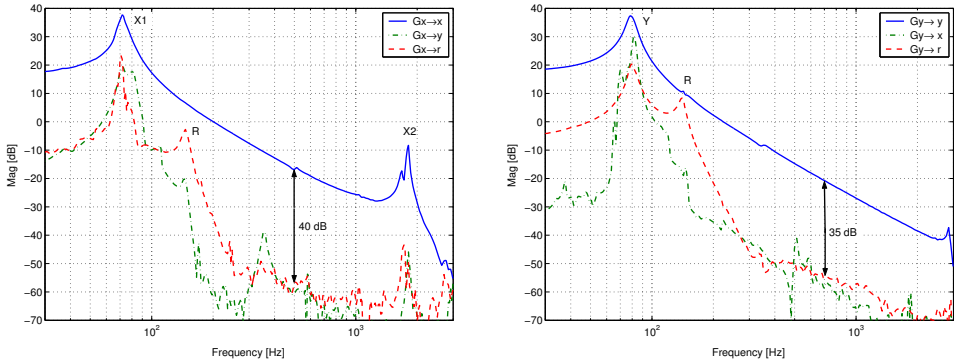

(a) Scanning responses (b) Tracking responses

Fig. 3. Plant frequency responses. Stronger coupling around the resonance modes.

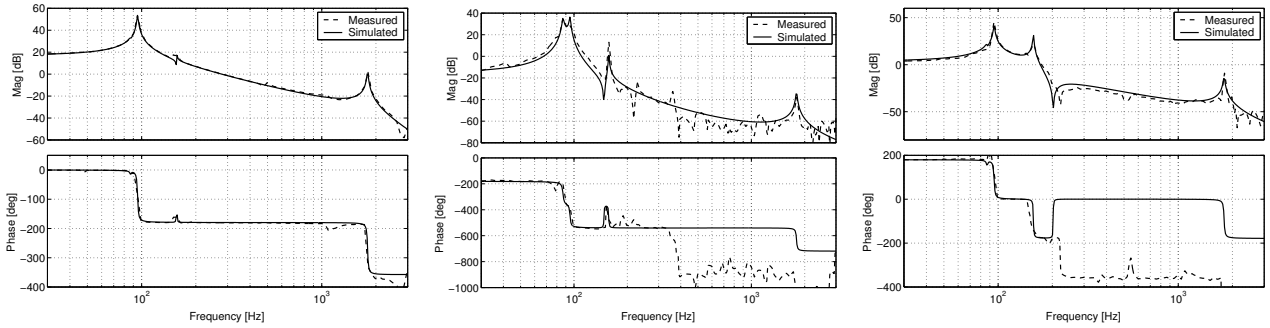

(a) Scanning → scanning (b) Scanning → tracking (c) Scanning → rotation

Fig. 4. Measured and modeled frequency responses: scanning to scanning, tracking, and rotation. Other cross transfer functions are obtained similarly but not shown here.

Cross-couplings are observed between scanning, tracking, and rotation. Some out-of-plane modes are also excited. Weak coupling is desired from the positioning control point of view. From Fig. 3, we see that the average gap between the direct and parasitic transfer functions are about 30∼40 dB for both the scanning and tracking directions. 40 dB gap implies that the motion in the tracking direction is ±500 nm when the scanning range is ±50 μm. This level of decoupling is clearly inadequate for achieving the positioning error of 1.5 nm 3σ.

2.2 System Identification

Four major in-plane modes are included in the plant model, forming a 3-input 3-output system. The transfer function from u_j to y_i, $G_{ij}(s)$, $i, j = 1, 2, 3$, can be written as

$$G_{ij}(s) = \sum_{n=1}^{4} \frac{K_{ij}^n}{s^2 + 2\zeta_n\omega_n s + \omega_n^2}, \tag{1}$$

where ω_n and ζ_n are the natural frequency and damping ratio of mode n respectively, and K_{ij}^n is the modal constant of mode n from u_j to y_i.

Before deriving a state-space expression for the above system, first consider the state-space representation of a single mode:

$$\begin{aligned} \begin{bmatrix} \dot{x}_1 \\ \dot{x}_2 \end{bmatrix} &= \begin{bmatrix} 0 & 1 \\ -\omega^2 & -2\zeta\omega \end{bmatrix} \begin{bmatrix} x_1 \\ x_2 \end{bmatrix} + \begin{bmatrix} 0 & 0 & 0 \\ b_1 & b_2 & b_3 \end{bmatrix} \begin{bmatrix} u_x \\ u_y \\ u_r \end{bmatrix}, \\ \begin{bmatrix} y_x \\ y_y \\ y_r \end{bmatrix} &= \begin{bmatrix} 1 & 0 \\ c_2 & 0 \\ c_3 & 0 \end{bmatrix} \begin{bmatrix} x_1 \\ x_2 \end{bmatrix}. \end{aligned} \tag{2}$$

Note that, without loss of generality, the first entry c_1 in the output matrix has been normalized to one. Then 5 independent parameters need to be determined: b_1, b_2, b_3, c_2, c_3.

From the measured frequency responses, we can actually obtain 9 transfer functions and hence 9 modal gains for each mode: $\begin{bmatrix} K_{11} & K_{12} & K_{13} \\ K_{21} & K_{22} & K_{23} \\ K_{31} & K_{32} & K_{33} \end{bmatrix}$. From the 9 measured parameters we need to determine 5 independent parameters in (2):

$$[b_1 \ b_2 \ b_3] = [K_{11} \ K_{12} \ K_{13}], \tag{3}$$

and

$$c_2 = \frac{K_{21}}{K_{11}} = \frac{K_{22}}{K_{12}} = \frac{K_{23}}{K_{13}}, \tag{4}$$

$$c_3 = \frac{K_{31}}{K_{11}} = \frac{K_{32}}{K_{12}} = \frac{K_{33}}{K_{13}}. \tag{5}$$

In (2), which element is to be normalized is not unique. A straightforward way is to select the output channel in which that mode has the highest gain and hence SNR, so that the estimation has the highest accuracy and least error propagation during gain scaling.

Combining the expressions for the four selected modes yields

$$\begin{aligned} \dot{\boldsymbol{x}} &= \boldsymbol{A}\boldsymbol{x} + \boldsymbol{B}\boldsymbol{u} \\ \boldsymbol{y} &= \boldsymbol{C}\boldsymbol{x} + \boldsymbol{D}\boldsymbol{u}, \end{aligned} \tag{6}$$

where $\boldsymbol{x} = [x_1 \ x_2 \ x_3 \ x_4 \ x_5 \ x_6 \ x_7 \ x_8]^T$, $\boldsymbol{u} = [u_x \ u_y \ u_r]^T$, $\boldsymbol{y} = [y_x \ y_y \ y_r]^T$. The measured and identified frequency responses are shown in Fig. 4. There is good agreement between measured and identified results. Some out-of-plane modes can

be seen in cross-coupling transfer functions. These modes can be viewed as model uncertainty in the following control design.

3. CONTROL DESIGN

3.1 Robust Control

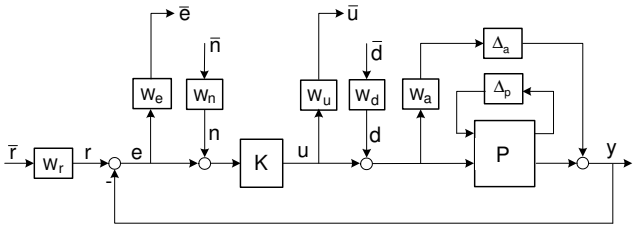

Fig. 5. μ-synthesis block diagram

State-space modeling has the capability of incorporating parametric and dynamic uncertainties for the following robust control design. Fig. 5 shows the block diagram for robust control design using μ-synthesis (Balas et al. [1995]). In that figure, P represents the three-input three-output plant as described by (6), K is the controller to be synthesized, r is the reference input, e is the tracking error, u is the control input to the plant, y is the plant output, and Δ_a and Δ_p are additive and parametric uncertainties of the plant. W_r, W_e, W_n, W_u, W_d, and W_a are weighting functions that must be selected to characterize the disturbance, noise, and design objectives. All variables having an overline are normalized disturbances or outputs.

To improve control performance, the designed closed-loop system is augmented by a tracking controller and a feedforward controller. A pure integrator is used as tracking controller for zero steady-state error (Young et al. [2006]), and the feedforward part is designed by the zero phase error tracking control (ZEPTC) technique (Tomizuka [1987]). They are all 3-by-3 diagonal matrices.

3.2 Simulation Results

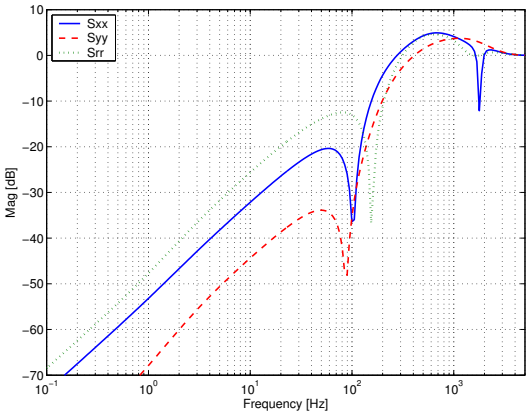

Fig. 6. Sensitivity of μ-synthesis

Fig. 6 shows the three sensitivities of the closed-loop system. Their closed-loop bandwidths are between 250∼500 Hz, and they are mainly limited by strong coupling and uncertainty. The integration action up to a low frequency (∼1 Hz) does not affect the stability of the μ-synthesized closed-loop plant.

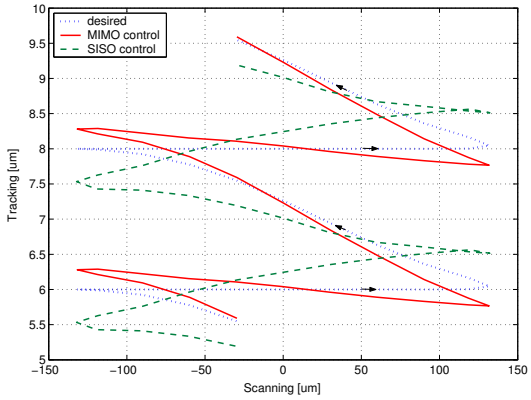

Fig. 7. Control performance

For comparison, a 3-by-3 diagonal controller is also designed via classical SISO loop shaping techniques. Each component consists of a PI compensator, a lowpass filter to reject high frequency noise, and a lead compensator for stability.

A 2-D reference trajectory is designed to mimic track scanning at a fixed speed followed by track seeking. The scanning range is ± 120 μm at 100 Hz with a track pitch of 2 μm. The rotation reference is set to zero. Fig. 7 shows the desired scanning pattern and the simulation results. The MIMO controller exhibits better performance than the SISO one because plant coupling has inherently been considered in the MIMO design. However, the errors at the beginning and end of each scanning are still big (∼250 nm). For further improvement, the closed-loop bandwidth should be extended and cross-coupling should be significantly reduced.

4. EXPERIMENTAL RESULTS

4.1 Iterative Learning Control

Experiments are conducted on the sled device using feedback information from both an LDV and capacitive sensors. Unfortunately, strong nonlinearities were observed when MIMO control is tried on the prototype system. The nonlinearities include, unmodeled dynamics like pitch and roll, coupling and the resulting stiction and friction between the moving and static parts, and the degraded signal quality. Taking these factors into account, iterative learning control (ILC) is applied rather than the previously simulated μ robust control. ILC is very effective in cancellation of any repeatable, linear or nonlinear, disturbances or errors (D. Bristow and Alleyne [2006]). In the experiments, only the tracking direction is controlled and evaluated under open-loop scanning. The scanning pattern r is a fixed sinusoidal. Fig. 8 shows the block diagram of a practical ILC architecture.

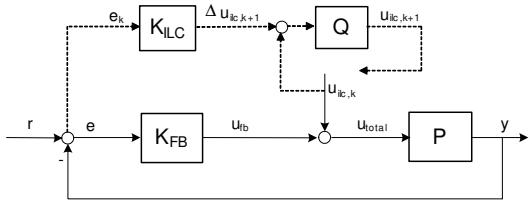

Fig. 8. Iterative learning control block diagram

In Fig. 8, K_{ILC} is the learning controller. Q is the lowpass filter doing tradeoff between performance and stability. The generation of $u_{\mathrm{ilc},k}$ is through iteration:

$$u_{\mathrm{ilc},k+1} = Q(u_{\mathrm{ilc},k} + \Delta u_{\mathrm{ilc},k+1}) = Q(u_{\mathrm{ilc},k} + \gamma L F e_k), \quad (7)$$

where F is the lowpass filter for noise filtering, L is the updating law, and γ is the step size which is normally less than one. A straightforward updating law is

$$L = \left(\frac{P}{1 + K_{\mathrm{fb}} P}\right)^{-1} = K_{\mathrm{fb}} + \frac{1}{P}. \quad (8)$$

The inversion of P can again be derived based on ZEPTC (Tomizuka [1987]).

4.2 Motion Measurement with Laser Doppler Vibrometer

In this experiment, the scanning pattern is a simple sinusoidal of ± 150 μm at 50 Hz. The tracking controller tries to keep the Y position at zero with a minimum tracking error. An LDV is used to measure the sled motion for feedback control.

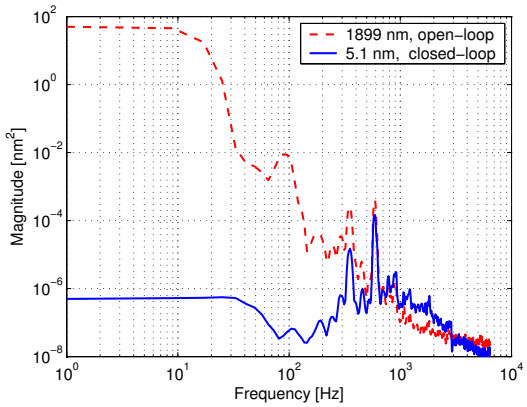

Fig. 9. Feedback control performance without scanning

Fig. 9 shows the feedback control performance when the system is not scanning and is only subject to sensor drift and noise and environmental vibrations. The closed-loop bandwidth is about 800 Hz. Note that all these disturbances and noises are nonrepeatable; Therefore, they cannot be cancelled by learning control which is intended for repeatable error compensation.

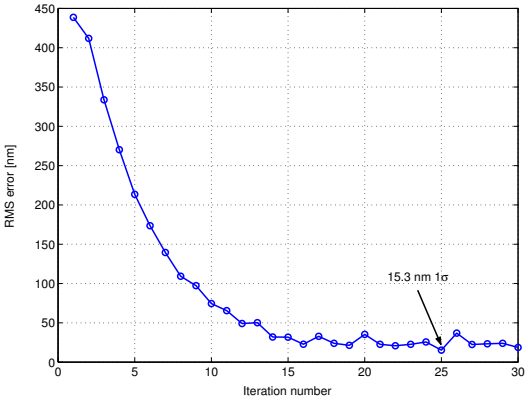

Fig. 10. Error convergence of ILC

Fig. 10 shows the error convergence process of iterative learning when the system is trying to follow the predefined scanning pattern. Before learning control, significant error is observed

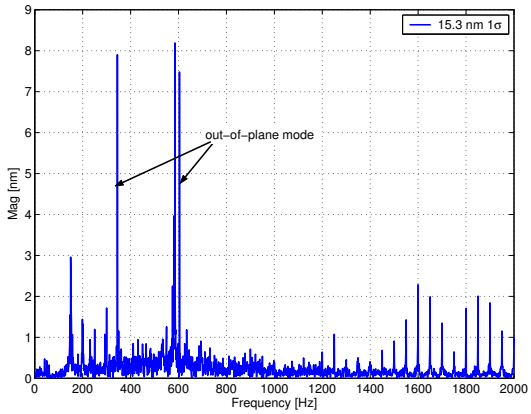

Fig. 11. Spectrum of the final tracking error

mainly due to the coupling from scanning to tracking. The error converges after about 15 iterations.

Fig. 11 shows the spectrum of the final tracking error after convergence. Two out-of-plane modes are observed in the middle frequency range. They are largely nonrepeatable and cannot be attenuated by learning control. Beyond the servo bandwidth and the passband of Q, higher harmonics of the scanning pattern are amplified slightly.

4.3 Development of MEMS Capacitive Sensor

This section describes the development of an integrated capacitive position sensor for measuring sub-nanometer linear and rotational displacements of probe sleds. The basic structure of the capacitive sensor is depicted in Figs. 12 and 13. Two sets of interdigitated electrodes on both the fixed (stator) and moving (rotor) sides form a variable capacitor (Hartwell et al. [2004]). A newly developed MEMS-fabricated rigid spacer, which is called 'post', was employed to guarantee precise control of gap spacing between the two substrates (Ramakrishnan et al. [2007]).

In each axis, normal (sine) and quadrature (cosine) sets of electrodes are required for unambiguous position decoding over the whole period ($= 2 \times (L + d)$). Then, for final position decoding, a standard method employs an arctan operation as illustrated on the right side of Fig. 13 in combination with an up-down counter to establish coarse position decoding.

For the required sensing electronics, the well-known continuous-time synchronous detection architecture was used because of its low noise performance and good flexibility (Baxter [1997]).

First, an elaborate sensor SNR model was developed to design the electrode layout (L, d and the number of electrodes) for a given sensing resolution requirement. The position sensing resolution target is 0.4 nm 1σ for a track pitch of 50 nm. With a

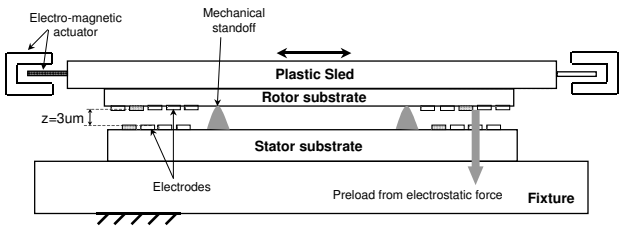

Fig. 12. Capacitive sensor structure for Probe storage: side view

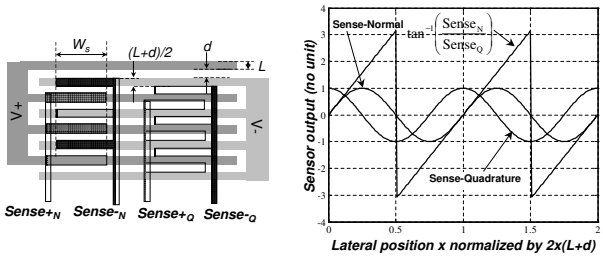

Fig. 13. Capacitive sensor structure for Probe storage: top view

sensor prototype design of 13 μm pitch and 3.46 mm^2 sensing area at 3 μm gap, the measured sensing noise was 0.2 nm 1σ, showing good agreement with the calculated value of 0.14 nm 1σ derived from the developed SNR model.

Then, solutions are proposed to enhance sensor linearity against rotational misalignment/disturbances during large strokes ($<$200 μm) and, at the same time, to provide an additional rotational position signal. The idea is to adopt another sensor set (X1&X2/Y1&Y2) in each axis(X/Y), which is symmetrically located with respect to the rotational axis as shown in Fig 14. An appropriate combination of these additional information provides a linear position signal (LPS) and a rotational position signal (RPS) which are in theory decoupled completely.

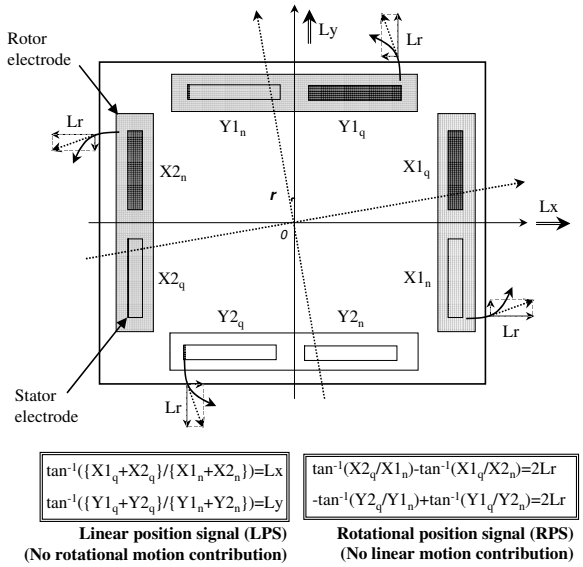

Fig. 14. Generation of linear position signal (LPS) and rotation position signal (RPS)

As is presented in Fig. 15 (a), the measured nonlinearity (maximum deviation from its linear fit divided by the whole range) in the LPS is 0.78% for 80 μm p-p stroke at 200 Hz. Lastly, Fig. 15 (b) shows the RPS measurement (in comparison with a differential LDV measurement as a reference) during rotational excitation at 200 Hz with offset linear actuators in plastic sled. When converted into an angular dimension, both signals agrees very well with each other, and hence we can conclude that the RPS information can be used for active rotation control purpose.

4.4 Control with Embedded Capacitive Sensor

In this experiment, a sled sample is integrated with the developed capacitive sensor for sled motion measurement and feed-

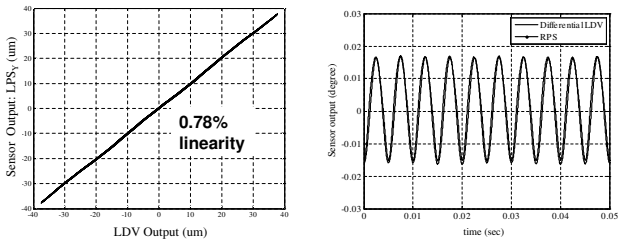

(a) (b)

Fig. 15. Experimental results for (a) sensor signal nonlinearity and (b) the rotational position signal

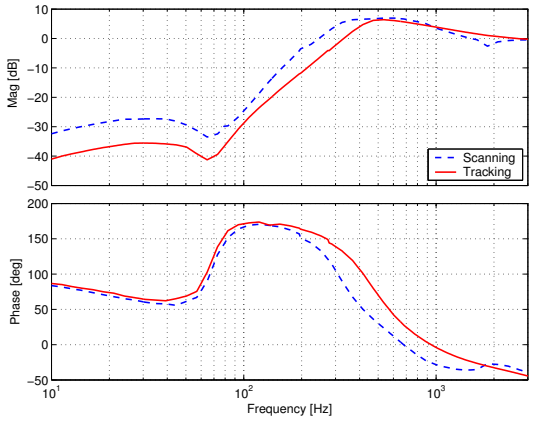

Fig. 16. Measured sensitivities for scanning and tracking

back control. The static part for holding the read/write heads is assembled with the moving media/sled part.

With the relative position information in the scanning and tracking directions, feedback controllers are designed for the two directions respectively. The measured sensitivities are shown in Fig. 16. As expected, the tracking sensitivity achieves higher bandwidth than the scanning one.

In this experiment, a 100 Hz scanning pattern is designed to achieve a constant velocity of 25 mm/s and a scanning range of $\pm$70 μm. The desired track position is constantly zero. In addition to feedback control, ILC is applied to further reduce the tracking error. Fig. 17 shows the scanning control performance. The remaining scanning error is still quite big. This is mainly due to the limited bandwidth of the scanning control and also the higher harmonics in the reference trajectory.

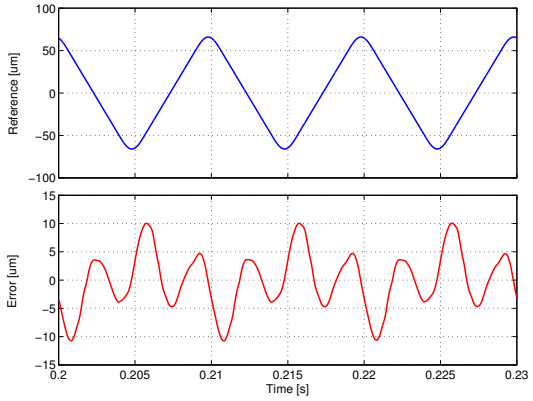

Fig. 17. Control effect of constant velocity scanning

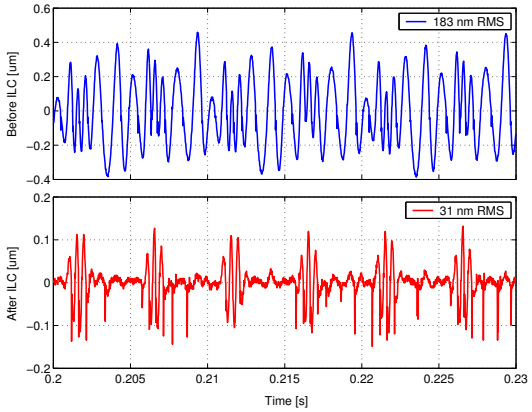

Fig. 18. Tracking control error

The tracking control performance is shown in Fig. 18. Significant improvement is made by ILC. After ILC, the biggest tracking error occurs right after the turn-around corners of the scanning trajectory, indicating limited bandwidth of tracking control.

The convergence process of ILC is shown in Fig. 19. Both the total RMS error and the errors at some frequencies are shown. Although the feedback control design is limited by the dynamics property of the plant, ILC can improve performance significantly as long as the plant is accurately modeled and the error is largely repeatable. As the scanning frequency becomes higher, improvement by ILC becomes less. A reasonable choice of the effective bandwidth for Q is between 2000 and 2500 Hz.

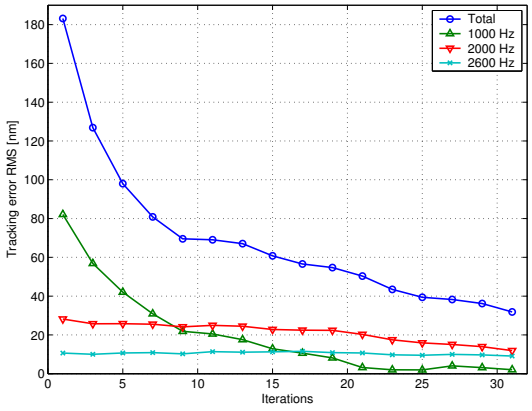

Fig. 19. Tracking error convergence

4.5 Rotation Control

In addition to tracking/seeking control, rotation control was also designed and tested. The rotation torque is weak due to the limited offset of the four magnetic keepers from their nominal center positions. Stiction/friction between the posts and the media have a stronger nonlinear effect on rotation than on linear motion. For these reasons, rotation control was implemented separately from scanning/tracking control.

Fig. 20 shows the rotation control effect when the sled is driven by a scanning trajectory at 120 Hz. D_x is the drive signal in the scanning direction, U_r is the rotation control signal, and E_r is the rotation angle. After rotation control is applied, the rotation error is reduced by about 60%.

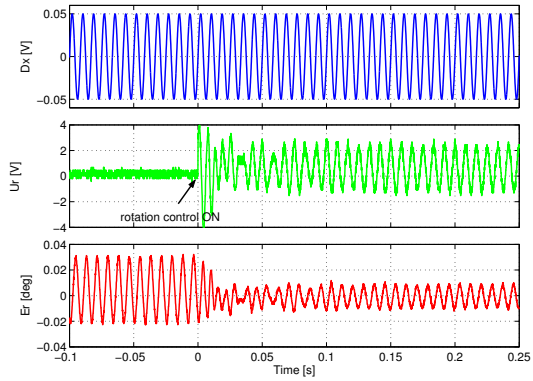

Fig. 20. Rotation control effect

5. CONCLUSION

Nanopositioning is a crucial aspect of probe storage due to its ultra-high areal densities. This paper describes the design, simulation and experimentation of a plastic scanner used for probe storage application. Experimental investigation demonstrates the feasibility of capacitive sensor and ILC in sled motion control. With the embedded capacitive sensor for position sensing and under closed-loop constant-velocity scanning at 100 Hz and ± 70 μm, the system achieves a tracking error of 31 nm 1σ. Performance improvement in scanning, tracking and rotation control is possible with further improvement in manufacturing and assembling of the device and hence the plant dynamics and sensing properties.

REFERENCES

H. J. Mamin, R. P. Ried, B. D. Terris, and D. Rugar. High-density data storage based on the atomic force microscope. In *Proceedings of the IEEE*, volume 87, 1999.

A. Sebastian, A. Pantazi, G. Cherubini, E. Eleftheriou, M. A. Lantz, and H. Pozidis. Nanopositioning for probe storage. In *Proc. of Amer. Control Conf.*, volume 5, pages 4181–4186, 2005.

G. J. Balas, J. C. Doyle, K. Glover, A. Packard, and R. Smith. *μ-Analysis and Synthesis Toolbox for use with MATLAB*. MUSYN Inc. and The MathWorks, Inc., USA, 1995.

P. M. Young, J. C. Morris, and H. T. Ho. μ-synthesis control with PI augmentation. In *Proc. of Amer. Control Conf.*, pages 1297–1302, 2006.

M. Tomizuka. Zero-phase error tracking algorithm for digital control. *ASME J. Dynamic Systems, Measurement and Control*, 109:65–68, March 1987.

M. Tharayil, D. Bristow, and A. Alleyne. A survey of iterative learning control. *IEEE Control Systems Magazine*, 26(3): 96–114, 2006.

P. Hartwell, R. Walmsley, D. Fasen, and S. Hoen. Integrated position sensing for control of xy actuator. In *IEEE Proc. of Sensors*, pages 1407–1410, Vienna, Austria, 2004.

N. Ramakrishnan, E. Johns, Y. Zhao, J. Kiely, M. Bedillion, and P. Chu. Sliding Contact Micro-Bearing for Nano-Precision Sensing and Positioning. *Transducers Conference*, Lyon, 2007.

L. Baxter. *Capacitive sensors: design and applications*. Piscataway, NJ: IEEE Press, 1997.